Available online at www.sciencedirect.com
ScienceDirect
Applied Thermal Engineering 29 (2009) 64–74
APPLIED THERMAL ENGINEERING
www.elsevier.com/locate/apthermeng

Numerical study of laminar heat transfer and pressure drop characteristics in a water-cooled minichannel heat sink

X.L. Xie, Z.J. Liu, Y.L. He, W.Q. Tao *

School of Energy and Power Engineering, Xi'an Jiaotong University, Xi'an, Shaanxi 710049, China

Received 2 October 2007; accepted 4 February 2008
Available online 9 February 2008

Abstract

With the rapid development of the information technology (IT) industry, the heat flux in integrated circuit (IC) chips cooled by air has almost reached its limit about 100 W/cm^2. Some applications in high technologies require heat fluxes well beyond such a limitation. Therefore the search of a more efficient cooling technology becomes one of the bottleneck problems of the further development of IT industry. The microchannel flow geometry offers large surface area of heat transfer and a high convective heat transfer coefficient. However, it has been hard to implement because of its very high pressure head required to pump the coolant fluid though the channels. A normal channel could not give high heat flux although the pressure drop is very small. A minichannel can be used in heat sink with a quite high heat flux and a mild pressure loss. A minichannel heat sink with bottom size of 20 mm × 20 mm is analyzed numerically for the single-phase laminar flow of water as coolant through small hydraulic diameters and a constant heat flux boundary condition is assumed. The effects of channel dimensions, channel wall thickness, bottom thickness and inlet velocity on the pressure drop, thermal resistance and the maximum allowable heat flux are presented. The results indicate that a narrow and deep channel with thin bottom thickness and relatively thin channel wall thickness results in improved heat transfer performance with a relatively high but acceptable pressure drop. A nearly-optimized configuration of heat sink is found which can cool a chip with heat flux of 256 W/cm^2 at the pumping power of 0.205 W. The nearly-optimized configuration is verified by an orthogonal design. The simulated thermal resistance agrees quite well with the result of conventional correlations method with the maximum difference of 12%.

Keywords: Heat transfer; Pressure drop; Minichannel; Heat sink; Numerical study

1. Introduction

With the rapid development of the IT industry, the heat flux in IC chips cooled by air has almost reached its limit about 100 W/cm^2. Some applications in high technologies require heat fluxes well beyond such a limitation. Therefore, the search for a more efficient cooling technology becomes one of the bottleneck problems of the further development of the IT industry. Microchannel liquid cooling is one of the candidates for this purpose. Microchannel cooling technology was first put forward in 1981 by Tuckerman and Pease [1], who employed the direct water circulation in microchannels fabricated in silicon chips. They were able to reach the highest heat flux of 7.9 MW/m^2 with the maximum temperature difference between substrate and inlet water of 71 °C. However, the penalty in pressure drop was also very high, i.e., 200 kPa with plain microchannels and 380 kPa with pin fin enhanced microchannels. Later, Philips [2] analyzed the heat transfer and fluid flow characteristics in microchannels in more details and provided formulations for designing microchannel geometries. Recently, Kandlikar et al. made a series studies on the direct liquid cooling technology by microchannels [3–5].

The microchannel flow geometry offers a large surface area of heat transfer and a high convective heat transfer

* Corresponding author. Tel./fax: +86 29 8266 9106.
E-mail address: wqtao@mail.xjtu.edu.cn (W.Q. Tao).

1359-4311/$ - see front matter © 2008 Published by Elsevier Ltd.
doi:10.1016/j.applthermaleng.2008.02.002

Nomenclature

A	area (m^2)
b_p	source term
c_p	specific heat capacity (J/Kg K)
D_h	hydraulic diameter of the fluid flow channel (m)
f	friction factor
H	height or thickness (m)
h	heat transfer coefficient (W/m^2 K)
L	channel length (m)
$\dot{m}$	total mass flow rate of coolant through channels (kg/s)
Nu	Nusselt number
n	number of cooling channels
p	pressure (Pa)
Δp	pressure drop (Pa)
Q	heat generation (W)
q	heat flux (W/m^2)
T	temperature (K)
res	residual
Re	Reynolds number
ΔT	temperature difference (K)
u,v,w	velocity of x, y, z, respectively (m/s)
U_{in}	inlet velocity (m/s)
$\dot{V}$	volumetric flow rate (m^3/s)
W	width of heat sink (m)
W_{pp}	pumping power (W)

Greek Symbols

ρ	density (kg/m^3)
μ	dynamic viscosity (kg/m s)
λ	thermal conductivity (W/m K)
η	fin efficiency
σ	Prandtl number
ν	kinematic viscosity of fluid (m^2/s)
ϕ	general variable
θ	thermal resistance (K/W)

Subscripts

b	bottom
c	channel
f	fluid
in	inlet
max	maximum value
s	solid
sf	surface available for heat transfer
w	wall

coefficient. However, it has been hard to implement in the compact/slim design of computers or consumer electronic devices. The major difficulty is driving water with high pressure head, which is required to pump the coolant fluid though the channels. A normal channel could not give such high heat flux although the pressure drop is very low. Thus, an idea comes into being that water-cooled minichannel can be used in heat sink with a high heat flux and a mild pressure loss. Here, by minichannels, we refer to the channels with their characteristic lengths within 0.2–3 mm [6]. In the following, a brief review on fluid flow and heat transfer of liquids in minichannels is presented.

Convective heat transfer and fluid flow in minichannel and their application in the cooling technology of electronic devices have attracted great attention of researchers in recent years. Gael et al. [7] indicated that the heat conduction in the walls of mini/microchannels makes the heat transfer multidimensional, and the axial heat conduction in the walls cannot be neglected. The surface roughness effects on pressure drop in single-phase flow in minichannels were investigated in Refs. [8–11]. Gao et al. [12] made experimental investigations of scale effects on hydrodynamics and the associated heat transfer in two-dimensional mini and microchannels with channel height ranging from 0.1 to 1 mm. Their results showed that the conventional laws of hydrodynamics and heat transfer can be applied to channels with height larger than 0.4 mm. Wang et al. [13] experimentally examined the frictional characteristics inside minichannels ($D_h = 0.198$–2.01 mm) with water and lubricant oil as the working fluids, and the tests were performed in both round and rectangular configurations. The test results indicated a negligible influence of viscosity on the friction factor if the hydraulic diameter is greater than 1.0 mm, and the measured data can be well predicted by the conventional correlation in both laminar and turbulent flow conditions. Agostini et al. [14] presented an experimental study of friction factor and heat transfer coefficient for a vertical liquid up flow of R-134a in minichannels. Downing et al. [15,16] experimentally investigated the single- and two-phase flow pressure drop and heat transfer characteristics in straight and miniature helical flow passages with R-134a as a working fluid. Debray et al. [17] performed the measurement of forced convection heat transfer coefficients in minichannels. Reynaud et al. [18] measured the friction and heat transfer coefficients in two-dimensional minichannels of 1.12–0.3 mm in thickness, and experimental results are in good agreement with classical correlations relative to channels of conventional size. From all the above-mentioned references, the following conclusions can be drawn: (1) In the liquid minichannels, the conventional physical and mathematical models for fluid flow and heat transfer with no-slip boundary conditions are still valid. (2) The friction factor and heat transfer correlations for conventional channels can also be used in minichannels as long as their relative surface roughness and relative channel wall thickness are not too high. The use of minichannels in the cooling technology of electronic devices can be found in the following references. Liu and Mui

[19] proposed a microprocessor package with water-cooling in which a narrow water jacket was used to cool a thermal spread attached to the silicon die backside for an efficient cooling. Schmidt [20] described a microprocessor liquid cooled minichannel heat sink and presented its performance as applied to a microprocessor (IBM Power 4) chip. Yazawa and Ishizuka [21] gave an analytic model for laminar flow and conducted a numerical study to optimize the channel in cooling spreader on a smaller and transient heat source. It was concluded that when small pumping power was available, a deeper channel with a thicker base was the best profile for the miniature channel coolers, and the best cooling performance was found at 0.0586 K/W for 0.03 W pumping power.

The aim of this study is to numerically design a water-cooling jacket which has relatively high heat transfer performance while keeping the pressure drop in an acceptable range. In the present paper, a multi-minichannel device has been designed and three-dimensional numerical simulation for its heat transfer and friction characteristics have been performed. In the following, the outlines of such a jacket will first be introduced and followed by its physical and mathematical models. Next, three-dimensional numerical results will be presented along with performance comparisons. Finally, some conclusions will be drawn.

2. Description of the designed cooling model

Fig. 1 shows a pictorial view of the suggested model. The unvaried total area being cooled is $W \times L$ with individual minichannel flow passage dimensions of $W_c \times H_c$. The wall separating the two channels is of thickness W_w and acts like a fin. The bottom plate thickness is H_b. The top cover is bonded, glued, or clamped to provide closed channels for liquid flow.

The channel dimensions W_c and H_c, the channel wall thickness W_w, the bottom plate thickness H_b, and the coolant flow velocity U_{in} are the parameters of interest in designing a minichannel heat sink. Their effects on thermal performance and pressure drop are examined in this paper. The maximum allowable temperature of the bottom surface and the acceptable pressure drop are the constraints. In addition, there are manufactures and cost constraints that need to be considered in any practical system design. However, in the following discussion, the manufacture and cost constraints are not taken into account.

3. Mathematical formulation and numerical methods

To analyze the thermal and flow characteristics of this model, the following assumptions are made:

(1) The flow is three-dimensional, incompressible, laminar and in steady-state.
(2) The effect of body force is neglected.
(3) The fluid thermophysical properties are constant and viscous dissipation is neglected.
(4) All minichannels are supposed to be identical in heat transfer and fluid flow; hence, one channel can be picked out as the representation for computation as shown in Fig. 2, where the coordinates system is indicated.

The governing equations based on the above assumptions are as follows.

Mass conservation equation:

$$\frac{\partial}{\partial x_i}(\rho u_i) = 0 \tag{1}$$

Momentum conservation equation:

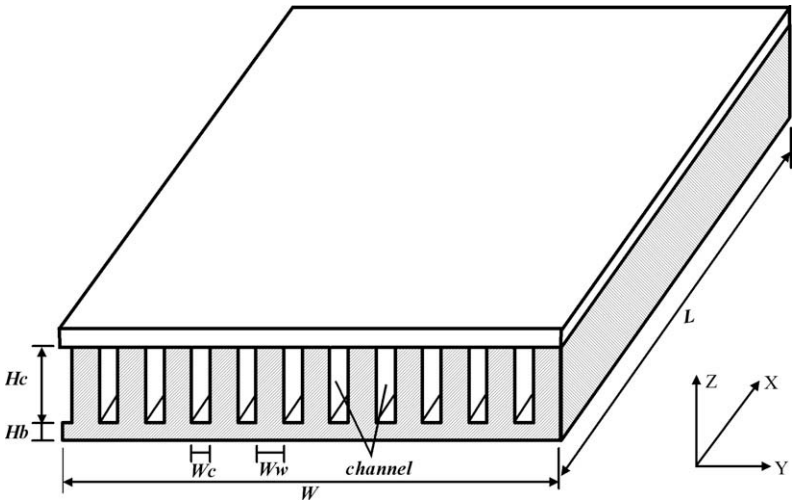

Fig. 1. Schematic view of the minichannel geometry for high heat flux cooling applications.

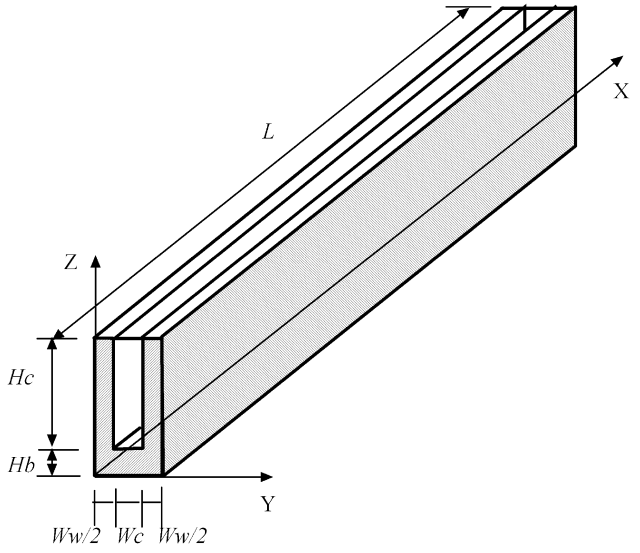

Fig. 2. Computational domain of the minichannel.

$$\frac{\partial}{\partial x_i}(\rho u_i u_j) = -\frac{\partial p}{\partial x_j} + \frac{\partial}{\partial x_i}\left(\mu\frac{\partial u_j}{\partial x_i}\right) + \frac{\partial}{\partial x_i}\left(\mu\frac{\partial u_i}{\partial x_j}\right), \quad j = 1,2,3 \tag{2}$$

Energy conservation equation:

$$\frac{\partial}{\partial x_i}(\rho u_i T) = \frac{\partial}{\partial x_i}\left[\left(\frac{\lambda}{c_p}\right)\frac{\partial T}{\partial x_i}\right] \tag{3}$$

In order to facilitate the investigation of channel geometry effects and channel thermal conductivity effect, the numerical simulation was conducted for the entire computational domain, with the solid region being treated as a special liquid. This implies that the computation is of conjugated type [22,23]. The no-slip hydraulic boundary condition of velocity is adopted for the solid wall, the inlet distribution is uniform for velocity at the channel inlet and the outlet boundary condition is considered of local one-way type [22,23]:

$$x = 0, \quad u = U_{in}, \quad v = w = 0 \tag{4}$$

$$x = L, \quad \text{the influence coefficient of the downstream equals zero} \tag{5}$$

$$u = 0, \quad v = 0, \quad w = 0, \quad \text{at solid walls} \tag{6}$$

The velocities in the solid region are everywhere zero which is automatically guaranteed by numerical solution algorithm for conjugated problem [22,23].

The thermal boundary conditions are given as follows. The left and right surfaces are the symmetry planes, and the boundary conditions are adiabatic:

$$y = 0, \quad \frac{\partial T}{\partial y} = 0 \tag{7}$$

$$y = W_c + W_w, \quad \frac{\partial T}{\partial y} = 0 \tag{8}$$

At the bottom position, the heat flux is given:

$$z = 0, \quad -\lambda_s\frac{\partial T}{\partial z} = q_w \tag{9}$$

The top surface is assumed to be adiabatic:

$$z = H_b + H_c, \quad \frac{\partial T}{\partial z} = 0 \tag{10}$$

At the inlet position, the inlet temperature of liquid is given to be constant, and the outlet boundary is considered of local one-way type [22,23]:

$$x = 0, \quad T = T_{in} \tag{11}$$

$$x = L, \quad \text{the influence coefficient of the downstream equals zero} \tag{12}$$

The discretization of the governing equations in the computational domain is performed on a staggered grid by using the finite volume method. A stability-guaranteed second-order difference scheme (SGSD) [24] is used to discretize the convective terms while the others are approximated by centre-difference approach. The SIMPLE solution algorithm is adopted to deal with the linkage between pressure and velocities, the details of which can be found in Refs. [22,23]. The deferred correction [23] is applied to deal with the high-order difference scheme for convective term. Then each of the discretized equations forms a tridiagonal matrix, which can be solved by the alternative direction iteration (ADI) with ease [22,23].

It should be noted that the problem at hand is a conjugated one in that both the fluid temperature and the temperature in the channel walls are to be simultaneously determined during the computation. For this purpose, the harmonic mean method is used to determine the diffusion coefficient at the control volume interface [22,23], and to keep the heat flux continuum at the interface the thermal conductivity at the different material regions should adopt individual values while the heat capacity of fluid is used for all the fluid and solid regions, because the nominal diffusion coefficient in the energy equation is λ/c_p, rather than λ itself [25]. By solving the problem in the conjugated manner, the boundary between the fins and the fluid becomes the inner interface of two neighboring control volumes, rather than the third kind of boundary of the fin. Thus the numerical method adopted in this paper can greatly save computational time.

It is well known that the channel width and the channel aspect ratio (H_c/W_c) have significant effects on the performance of minichannel heat sink. In order to get better thermal performance and acceptable mild pressure drop, the

Table 1
Range of test parameters

Parameters	Range
U_{in} (m/s)	0.1–1.5
W_c (mm)	0.5–0.8
H_c (mm)	2–6
W_w (mm)	0.1–0.5, 0.8, 1.0
H_b (mm)	0.1–0.8, 1.0

effects of the channel geometry and inlet velocity are investigated parametrically, and the range of the geometric parameters and the inlet velocity are shown in Table 1. The width of channel from 0.5 to 0.8 mm can be easily manufactured with current conventional fabrication technology and H_c should not be very large for the consideration of compactness and ease of manufacture. The hydraulic diameter D_h of the fluid flow channel and Reynolds number Re are defined as

$$D_h = \frac{4W_cH_c}{2(W_c + H_c)} \tag{13}$$

$$Re = \frac{U_mD_h}{v} \tag{14}$$

where U_m is the mean fluid velocity in minichannel which is equal to inlet velocity U_{in}, and v is the kinematic viscosity of fluid.

Definition of overall thermal resistance θ is shown in equation:

$$\theta = \frac{T_{max} - T_{in}}{Q} \tag{15}$$

$$Q = q \times A_b \tag{16}$$

where T_{max} is the maximum bottom temperature, T_{in} is the inlet fluid temperature, Q is the total heat generation, q is the bottom heat flux, and A_b is the whole heating area of heat sink.

When the Reynolds number is less than 2300, the flow regime in the minichannel is considered laminar. All the Reynolds numbers are less than 2300 with the parameters listed in Table 1. The inlet temperature of water is 300 K. The thermophysical properties of water at 40 °C are used in the numerical simulation. The material of heat sink is pure copper. The bottom dimension is 20 mm × 20 mm, which was determined according to the conventional chip sizes. Since the channel width spans a quite large variation, the gird systems are different for individual case, and the finest grid system adopted in the computation has nodes as large as 840,000.

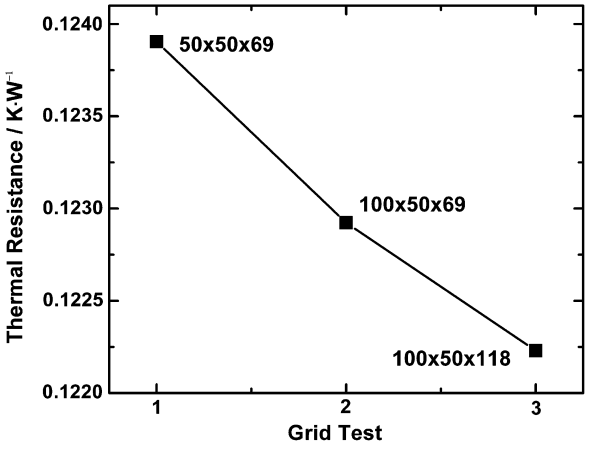

Fig. 3. Grid test for minichannel with $W_c = 0.5$ mm, $H_c = 5$ mm, $W_w = 0.5$ mm, $H_b = 1$ mm, and $U_{in} = 1$ m/s.

The grid independence examination of the numerical solution is illustrated in Fig. 3, where the thermal resistance is displayed. The parameters are W_c=0.5 mm, H_c=5 mm, $W_w = 0.5$ mm, $H_b = 1$ mm, and $U_{in} = 1$ m/s, respectively. The deviation between case 2 (100 × 50 × 69) and case 3 (100 × 50 × 118) is very small (less than 1%), so grid system of case 2 is adopted for the parameter combination mentioned above. During the iterative solution process if the relative deviation between two consecutive iterations is less than the specified small value ε_ϕ, the iteration is considered converged:

$$\max(|\phi^n_{i,j,k} - \phi^{n-1}_{i,j,k}| / |\phi^n_{i,j,k}|) < \varepsilon_\phi \tag{17}$$

where ϕ represents the variables u, v, w and t. $\varepsilon_\phi = 10^{-7}$ is used in this paper.

4. Results and discussion

Supplied pumping power W_{pp} to generate the flow is defined in equation:

$$W_{pp} = n \cdot \dot{V} \cdot \Delta p \tag{18}$$

where n is the number of cooling channel, which is equal to the integer part of $\frac{W}{W_w+W_c}$, $\dot{V}$ is the volumetric flow rate and Δp is the pressure drop through the heat sink.

The effects of channel width W_c, channel height H_c, bottom plate thickness H_b, channel wall thickness W_w and inlet velocity U_{in} are parametrically studied. The numerical results will first be presented about the influences of those parameters on the water pressure drop Δp through the cooling device and the thermal resistance θ in the device. When the pressure drop Δp and thermal resistance θ are studied, the bottom heat flux q_w is assumed to be 100 W/cm^2, while when the effect on the maximum heat flux q_{max} is concerned, the maximum temperature difference ΔT is taken as 50 °C. Attention is then turned to seek the nearly-optimized configuration of the minichannel and the corresponding geometries are proposed. Finally some conclusions are drawn.

In the parametric study only one parameter is varied while all the others are kept constant, and the values of other parameters are initiated at first. After the effect of one parameter has been investigated and the best value of the parameter has been obtained with other parameters remained constant, the best value found in such a way is assumed to be the best value for all other parameter combinations and is used in the successive study for other parameters. The rationality of such practice will be discussed later.

4.1. Effect of channel height

The relations of the pressure drop and pumping power with channel height are shown in Fig. 4. The computations are conducted for the case of inlet velocity of 1 m/s, bottom

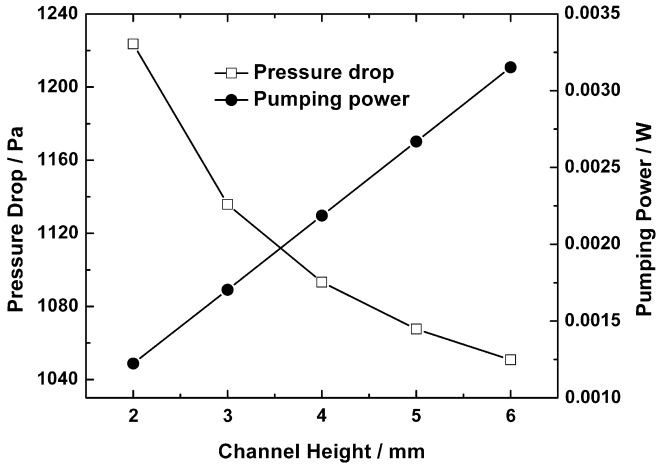

Fig. 4. Effect of channel height on pressure drop and pumping power.

plate thickness of 1 mm, channel wall thickness and channel width of 0.5 mm.

As shown in Fig. 4, the pressure drop decreases with the increase in channel height. Flow rate per channel increases linearly with the increase in channel height at constant inlet velocity, while the corresponding pressure loss decreases mildly. As can be observed in the figure, the pressure drop decreases about 15% from channel height of 2–6 mm. The pumping power increases with the increase in channel height, and the slope of the pumping power vs. channel height shows a linear variation.

Fig. 5 shows that the variation of the thermal resistance with channel height has the similar trend as the pressure drop vs. channel height. It can be observed from the figure that for the case studied further increase in the channel height make no contribution to the increase of the maximum heat flux. The maximum heat flux deviation is less than 4% for the channel height of 5 and 6 mm. So in the following discussion the channel height of 6 mm will be chosen as the optimum value.

4.2. Effect of channel width

When effect of channel width is considered, the computations are conducted for the case of inlet velocity of 1 m/s, channel height of 6 mm, channel wall thickness of 0.5 mm and bottom plate thickness of 1 mm. Here the purpose is to examine the maximum heat flux with the change of channel width. Thus as indicated above, the constraint of temperature difference 50 K is applied. The variations of pressure drop and pumping power with channel width are shown in Fig. 6. They both have the same variation trend and both decrease with the increase of channel width. The maximum heat flux also decreases with the channel width while the thermal resistance varies in the opposite direction as shown in Fig. 7. From the variation of thermal resistance with channel dimensions shown in Figs. 5 and 7, it is found that the narrow and deep channel is better for heat transfer, in spite of higher pressure drop penalty. To keep a reasonable balance between pressure drop and heat flux, the channel width of 0.5 mm will be chosen as the optimum value in the following discussion.

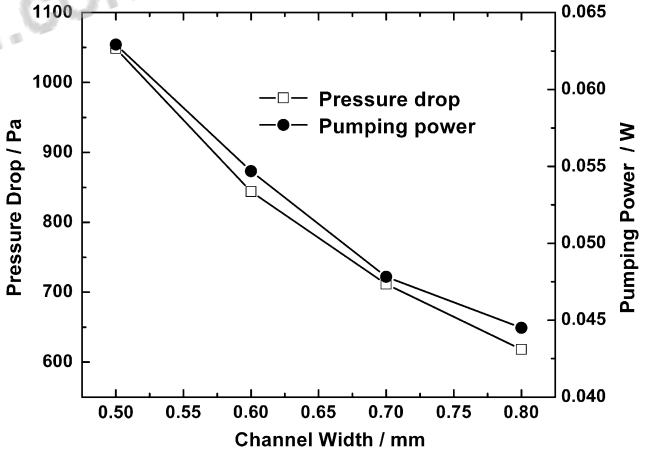

Fig. 6. Effect of channel width on pressure drop and pumping power.

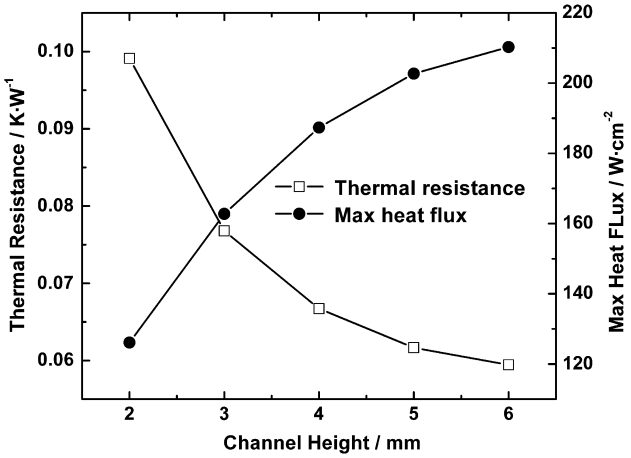

Fig. 5. Effect of channel height on thermal resistance and max heat flux.

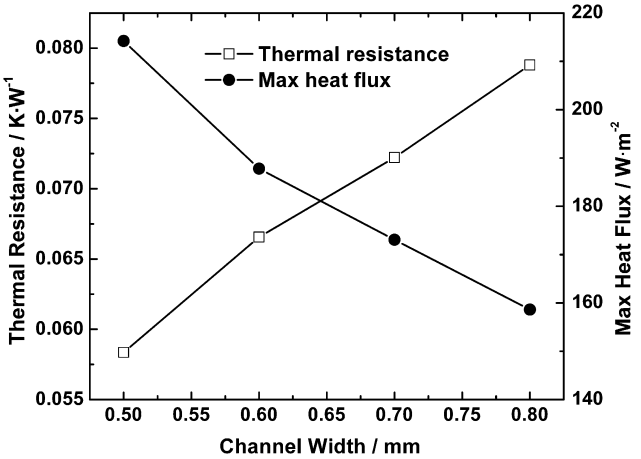

Fig. 7. Effect of channel width on thermal resistance and max heat flux.

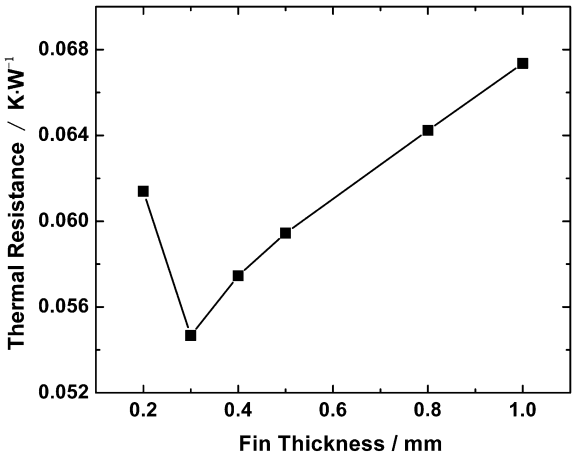

Fig. 8. Effect of channel wall thickness on thermal resistance.

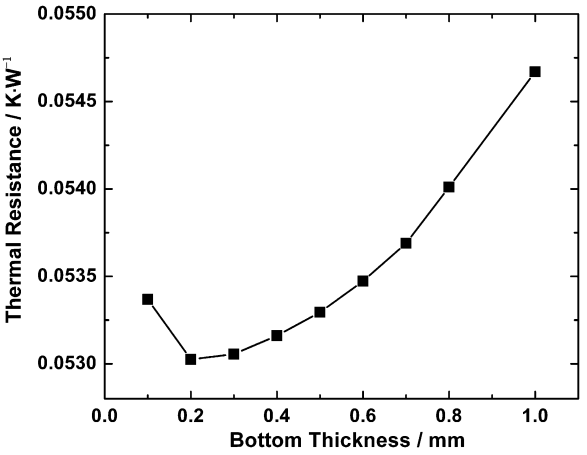

Fig. 9. Effect of bottom plate thickness on thermal resistance.

4.3. Effect of channel wall thickness

Fig. 8 represents the variation trend of thermal resistance vs. channel wall thickness. The computations are conducted for the case of inlet velocity of 1 m/s, channel height of 6 mm, channel width of 0.5 mm and bottom plate thickness of 1 mm. Numerical results show that the channel wall thickness has significant effect on the thermal resistance, and there is a turning point of channel wall thickness at which the thermal resistance reaches its minimum. This variation pattern can be analyzed as follows. The heat transfer process from the bottom to the cooling water of the channel includes two thermal resistances in series: the conductive thermal resistance through the channel wall and the convective thermal resistance of the side wall, which is fixed at the given inlet velocity and the given side wall surface area. When the channel wall thickness W_w is too narrow the conductive thermal resistance predominated and the increase in W_w reduces the conductive thermal resistance, hence, the total thermal resistance. However, further increase in W_w leads to the significant increase in the total heat transfer rate entering the computational unit for the fixed heat flux condition, and this causes the increase in T_{max} in order to transfer the increased total heat transfer rate at the fixed convective heat transfer condition. The turning point at the channel wall thickness of 0.3 mm makes the best thermal performance. So it is considered that the thickness of 0.3 mm is the optimum one of the channel walls.

4.4. Effect of bottom plate thickness

Fig. 9 shows the effect of bottom plate thickness on thermal resistance. The computations are conducted for the case of inlet velocity of 1 m/s, channel height of 6 mm, channel wall thickness of 0.3 mm and channel width of 0.5 mm. Pressure drop and pumping power are remained unchanged for each inlet velocity due to the fixed channel dimensions. From the figure it can be seen that the thermal resistance first decreases with the increase of bottom plate thickness, reaches its minimum at 0.2 mm and then increases with the increase of bottom plate thickness. For the case studied bottom plate thickness of $H_b = 0.2$ mm is the turning point when the effect of bottom plate thickness is considered. The heat transfer rate entering into the bottom surface of H_b is transferred through two ways: one-way is the heat conduction from the bottom surface to the top surface of H_b and the other is from the bottom surface to the two side walls of the computational unit. The first part increases with the decrease of H_b, while the second part decreases with the decrease of H_b. The above-mentioned variation trend is resulted from the balancing between the heat conduction of the two parts. In the following discussion the bottom thickness of 0.2 mm will be chosen as the optimum value.

From the above discussion about the influences of parameters of interest on the pressure drop and thermal resistance, we can obtain a nearly-optimized configuration of the heat sink as follows: $W_c = 0.5$ mm, $H_c = 6$ mm, $H_b = 0.2$ mm, $W_w = 0.3$ mm. For this nearly-optimized configuration there are total 25 channels for the fixed width of the heat sink. To verify the numerical results the present authors have conducted additional numerical simulation based on the orthogonal design method, the details of which can be found in Montgomery [26] and Liu [27]. The factors and their levels have been shown in Table 2 where factors A, B, C and D are the channel height, the channel width, the channel wall thickness and the bottom

Table 2
Factors and their levels

Levels	Factors			
	A H_c (mm)	B W_c (mm)	C W_w (mm)	D H_b (mm)
1	2	0.5	0.1	1.0
2	4	0.6	0.3	0.2
3	5	0.7	0.7	0.5
4	6	0.8	1.0	0.8

Table 3
Arrangement of test using L_{16} (4^5) orthogonal array

Column No. Factors Run	1	2	3	4	5
	A	*B*	*C*	*D*	Blank
	H_c (mm)	W_c (mm)	W_w (mm)	H_b (mm)	
1	1	2	3	2	/
2	3	4	1	2	/
3	2	4	3	3	/
4	4	2	1	3	/
5	1	3	1	4	/
6	3	1	3	4	/
7	2	1	1	1	/
8	4	3	3	1	/
9	1	1	4	3	/
10	3	3	2	3	/
11	2	3	4	2	/
12	4	1	2	2	/
13	1	4	2	1	/
14	3	2	4	1	/
15	2	2	2	4	/
16	4	4	4	4	/

Table 4
Analysis of the numerical experiment results

Run	Factors				
	A H_c (mm)	*B* W_c (mm)	*C* W_w (mm)	*D* H_b (mm)	Results θ(K·W^{-1})
1	1	2	3	2	0.115725
2	3	4	1	2	0.096020
3	2	4	3	3	0.085995
4	4	2	1	3	0.076881
5	1	3	1	4	0.097882
6	3	1	3	4	0.062047
7	2	1	1	1	0.069161
8	4	3	3	1	0.069927
9	1	1	4	3	0.126800
10	3	3	2	3	0.068901
11	2	3	4	2	0.090063
12	4	1	2	2	0.052746
13	1	4	2	1	0.108380
14	3	2	4	1	0.076046
15	2	2	2	4	0.066525
16	4	4	4	4	0.078836
$\overline{T_1}$	0.112197	0.077688	0.084986	0.080878	
$\overline{T_2}$	0.077936	0.083794	0.074138	0.088638	
$\overline{T_3}$	0.075753	0.081693	0.083424	0.089644	
$\overline{T_4}$	0.069597	0.092308	0.092936	0.076323	

plate thickness, respectively. The arrangement of test using L_{16} (4^5) orthogonal array can be seen in Table 3. This table is copied from [27], in which five factors can be considered with each parameters has four levels. Since in our problem there are only four factors, the last column of Table 3 is empty (blank). There are totally 16 combinations of the four factors should be computed. The results of the thermal resistance are listed in the last column of Table 4. In the table $\overline{T_i}$ represents the average effect of *i*th level of a factor. From Table 4 it can be directly seen that the smallest thermal resistance (0.052746 K/W) is reached by No.12. It is to be noted that the case 12 is also the parameter combination of the nearly-optimized configuration found in the previous computation, which can be expressed by the level selection of 4-1-2-2 of the four factors in order.

A careful inspect of Table 4 may find that for factor *D* the average effect of Level 4 ($\overline{T_4} = 0.076323$) is less than that of Level 2 ($\overline{T_2} = 0.088638$), while Level 2 of factor *D* is incorporated in the optimized combination. In order to confirm the validity of the selection, the present authors have conducted additional numerical simulation to compare the results of the two parameter combinations. The former three factors take the levels of 6, 0.5 and 0.3 mm, respectively, while factor *D* takes Level 2 and Level 4, i.e., the combination between 4-1-2-2 and 4-1-2-4 is conducted. It is found that the thermal resistance of 4-1-2-2 is less than that of the combination of 4-1-2-4.

It is interesting to note that the present authors also have made another design of experiment (DOE) in which the four levels of the factor *D* is selected as 0.1, 02, 03, and 0.4 mm. The results once again confirmed that the combination of 4-1-2-2 is the best one.

4.5. Effect of inlet velocity

Simulations of inlet velocity effect are conducted for this nearly-optimized configuration and the results are presented in Figs. 10–12. Pressure loss varies from about 70 Pa at inlet velocity of 0.1 m/s to about 1817 Pa at inlet velocity of 1.5 m/s, while pumping power from 5.3×10^{-4} to 0.205 W. The variations of thermal resistance and the maximum heat flux with inlet velocity are shown in Fig. 11. Thermal resistance decreases with the increase of inlet velocity, while the maximum heat flux increases. The thermal resistance decreases with the increase of inlet velocity, and its slope decreases gradually. The increase in inlet velocity can reduce the convective thermal resistance which is only a part of the total thermal resistance. With the decrease in the convective thermal resistance the

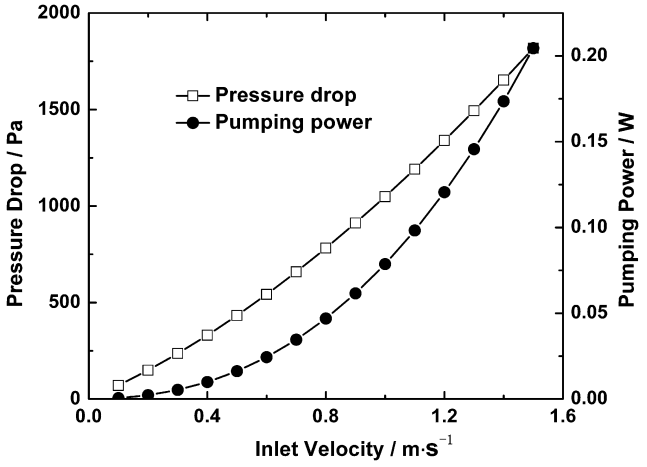

Fig. 10. Pressure drop and pumping power by inlet velocity based on the nearly-optimized channel geometry.

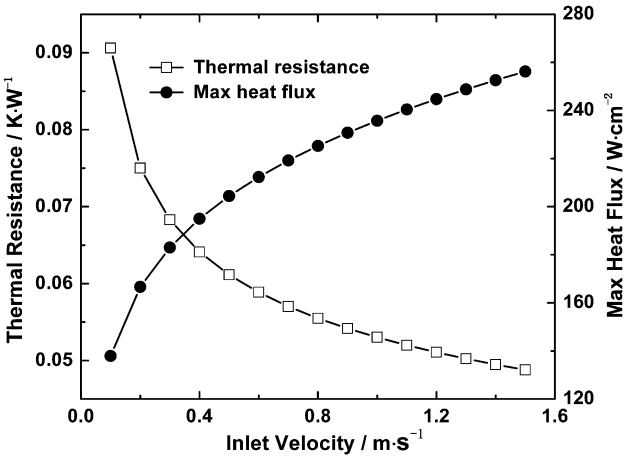

Fig. 11. Thermal resistance and maximum heat flux by inlet velocity based on the nearly-optimized channel geometry.

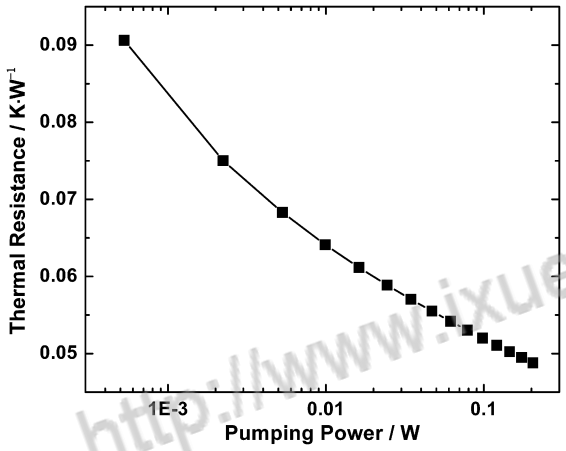

Fig. 12. Thermal resistance by pumping power based on the nearly-optimized channel geometry.

conductive part becomes more and more important, and this leads to the less effect of the reduction in the convective thermal resistance. Therefore, at relative high inlet velocity the gain in the total thermal resistance reduction is obtained with high penalty of pressure drop. The thermal resistance is 0.0488 K/W and the maximum heat flux is 256 W/cm^2 at inlet velocity of 1.5 m/s. At the low inlet velocity of 0.1 m/s, the thermal resistance and the maximum heat flux are 0.091 K/W, and 137 W/cm^2, respectively. For this nearly-optimized configuration, the relationship between thermal resistance and pumping power under the above conditions is presented in Fig. 12.

4.6. Comparison with results predicted by correlations

As mentioned in the introduction section, conventional correlations can be used to predict the flow and heat transfer characteristics in minichannels. So conventional Darcy friction factor f can be used to obtain pressure drop Δp, or vice versa

$$f = \frac{\Delta p}{\frac{\rho U_{in}^2}{2}} \frac{D_h}{L} \tag{19}$$

For the determination of Nusselt number, Nu, we use the correlation in terms of channel aspect ratios (α_s) obtained by Kim and Kim [28]:

$$Nu = 2.253 + 8.164\left(\frac{\alpha_s}{\alpha_s + 1}\right)^{1.5} \tag{20}$$

Convective heat transfer coefficient h can be obtained from Nusselt number:

$$h = \frac{Nu\lambda_f}{D_h} \tag{21}$$

where D_h is hydraulic diameter and λ_f is the thermal conductivity of fluid.

The heat sink can be analyzed as a two-dimensional flow through narrow rectangular channels with a constant heat flux boundary condition at the bottom of plate, and capacity resistance and convective resistance were considered in Ref. [29]. Here conductive resistance is also included when the thickness of bottom plate is taken into account. Thermal resistance θ including three thermal resistance terms in series is expressed by

$$\theta = \frac{1}{hA_{sf}} + \frac{1}{\dot{m}c_p} + \frac{1}{\lambda_s A_b / H_b} \tag{22}$$

where $\dot{m}$ is the total mass flow rate of coolant through channels and A_b is the bottom area. The inclusion of the capacity resistance comes from the fact that the definition of the total thermal resistance θ is based on the temperature difference of $(T_{max} - T_{in})$ (see Eq. (15)).

The surface area available for heat transfer, A_{sf}, can be written as [30]:

$$A_{sf} = nW_c L + 2n\eta H_c L \tag{23}$$

where η is the fin efficiency which is expressed as

$$\eta = \frac{\tan h(mH_c)}{mH_c} \tag{24}$$

where H_c is the height of channels and m is defined as

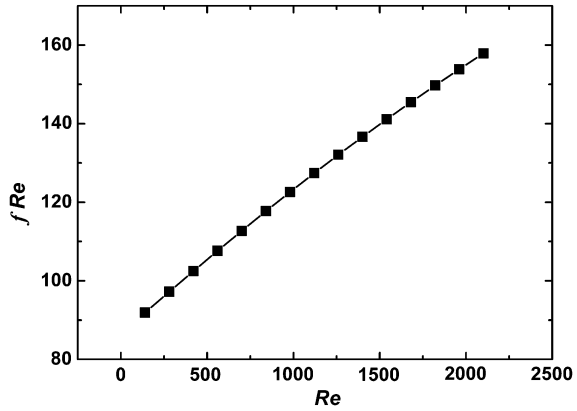

Fig. 13. Relationship between fRe and Re.

$$m = \sqrt{\frac{2h}{\lambda_s W_w}} \tag{25}$$

with the assumption of $L \gg W_w$.

Comparison calculations were performed between three-dimensional numerical simulation and correlation approach as mentioned above. Fig. 13 gives the relationship between fRe and Re. The results show that fRe increases with the increase of Re. For laminar channel flow in conventional size, it is well known that fRe should be a constant for the fully developed region. However, the minichannel flow here is in the developing region because of the uniform distribution of inlet velocity, which is the reason why the numerical predictions vary with Re. To verify this understanding the present authors have conducted additional numerical calculations by posing periodic boundary conditions at the channel inlet and outlet. It is found that such predicted values of fRe do not vary with Re.

Fig. 14 displayed the effect of inlet velocity on thermal resistance for the nearly-optimized configuration based on the two methods, respectively. The two curves of thermal resistance shown in Fig. 14 are in good agreement with each other with the maximum difference about 12%. However, the two curves have an intersection point, and the curve of correlation trends to reach a limitation, while the other still has the potential to reduce thermal resistance. This difference can be understood as follows. For the correlation approach, because the aspect ratio (α_s) of the nearly-optimized minichannel configuration is a constant, according to Eqs. (20) and (21) the Nusselt number (Nu) and convective heat transfer coefficient (h) are constant, then the first term of Eq. (22) does not vary with the inlet velocity. Also, the third term has no change with the fixed bottom plate thickness. Hence, inlet velocity or flow rate can only effect the second term of thermal resistance θ in Eq. (22), which reduces to limit value of zero with the increase of flow rate, so the limitation of thermal resistance θ is the constant sum of the first term and the third term of Eq. (22). Actually, due to the uniform distribution of inlet velocity, the flow in minichannel is not developed fully, therefore entrance effect should be taken into account, so Nusselt number (Nu) and convective heat transfer coefficient (h) should not be constant, and flow rate has influence on them. Both of them increase with the increase of inlet velocity, so the first term of thermal resistance and the total thermal resistance reduce with the increase of inlet velocity.

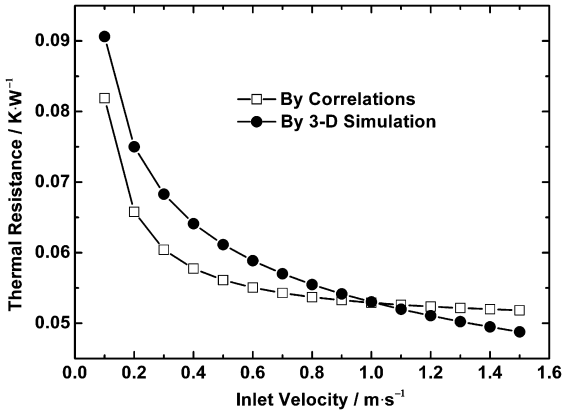

Fig. 14. Results comparison on the effect of inlet velocity on thermal resistance.

It should be emphasized that the quite good agreement does not necessary mean that the three-dimensional numerical simulation is not useful, rather, it is the three-dimensional numerical simulation that can account for the complicated effects of different factors and give a clear physical understanding of the heat transfer and fluid flow process. And only when the comparison between the prediction of the three-dimensional simulation and the correlation prediction ensures their agreement, the correlation method then can be used in the preliminary design of the cooling devices.

5. Conclusions

The heat transfer and pressure drop characteristics for single-phase laminar flow in minichannel heat sinks are analyzed in the present paper. The results are presented for a chip with an active cooling area of 20 mm × 20 mm. From the results and analysis, following conclusions can be obtained:

(1) Pressure drop, an important parameter for minichannel heat sink design is a strong function of the channel geometry. From heat transfer, a narrow and deep channel is better than that of a wide and shallow channel, in spite of the high pressure drop penalty. To keep a reasonable balance between pressure drop and heat transfer, optimized study should be conducted for every given case.

(2) Both channel wall thickness and bottom plate thickness have an optimum value at which thermal resistance reaches its minimum according to the limited bottom surface area.

(3) A nearly-optimized configuration is obtained for the heat sink with bottom size of 20 mm × 20 mm. For this heat sink the maximum heat flux reaches about 256 W/cm^2 under the constraint of temperature difference 50 K with inlet velocity of 1.5 m/s, the corresponding thermal resistance is 0.0488 K/W and pumping power is 0.205 W. Even at lower inlet velocity of 0.1 m/s, the thermal performance is also quite good with thermal resistance of 0.091 K/W, pumping power of 5.3×10^{-4} W and the maximum heat flux of 137 W/cm^2. The orthogonal analysis has verified the nearly-optimized configuration to be the best one in the research ranges of parameters.

(4) A good agreement is obtained from the comparison between the thermal resistance predicted by conventional correlations and numerical simulations with the maximum difference about 12%. However, numerical simulations can predict the entrance effect on pressure drop and thermal performance for the uniform distribution of inlet velocity, while correlation method based on the fully developed profiles fails to reveal such characteristics.

Acknowledgement

This work has been supported by the National Natural Science Foundation of China (Grant Nos. 50636050, 50425620).

References

[1] D.B. Tuckerman, R.F.W. Pease, High performance heat sink for VLST, IEEE Electron Dev. Lett., EDL-2 5 (1981) 126–129.
[2] R.J. Philips, Forced convection, liquid cooled, microchannel heat sinks, M.S. Thesis, Department of Mechanical Engineering, Massechussetts Institute of Technology, Cambridge, 1987.
[3] S.G. Kandlikar, H.R. Upadhye, Optimization of microchannel geometry for direct chip cooling using single-phase transfer, in: Proceedings of Microchannels and Minichannels-2004, ASME, NY, 2004, pp. 679–614.
[4] S.G. Kandlikar, W.J. Grande, Evaluation of single-phase flow in microchannels for high flux CHIP cooling – thermohydraulic performance enhancement and fabrication technology, in: Proceedings of Microchannels and Minichannels-2004, ASME, NY, 2004, pp. 67–76.
[5] S.G. Kandlikar, High flux heat removal with microchannels – a roadmap of challenges and opportunities, in: Proceedings of Microchannels and Minichannels-2005, ASME, Toronto, 2005, pp. 1–10.
[6] S.G. Kandlikar, Heat transfer mechanisms during flow boiling in microchannels, J. Heat Transfer 126 (2004) 8–16.
[7] M. Gael, P. Isabelle, M. Denis, Mini- and microchannels: influence of axial conduction in the walls, Int. J. Heat Mass Transfer 47 (2004) 3993–4004.
[8] D.J. Schmitt, Experimental investigation of surface roughness microstructures and their effects on pressure drop characteristics in rectangular minichannels, M.S. Thesis, Department of Mechanical Engineering, Rochester Institute of Technology, 2004.
[9] D.J. Schmitt, S.G. Kandlikar, Effects of repeating microstructures on pressure in rectangular minichannels, in: Third International Conference on Microchannels and Minichannels, Toronto, Canada, 2004, June 13–15.
[10] Z.Y. Guo, Z.X. Li, Size effect on microscale single-phase flow and heat transfer, Int. J. Heat Mass Transfer 46 (2003) 149–159.
[11] Z. Li, Y.L. He, G.H. Tang, W.Q. Tao, Experimental and numerical studies of liquid flow and heat transfer in microtubes, Int. J. Heat Mass Transfer 50 (2007) 3447–3460.
[12] P.Z. Gao, S.L. Person, M. Favre-Marinet, Scale effects on hydrodynamics and heat transfer in two-dimensional mini and microchannels, Int. J. Therm. Sci. 41 (2002) 1017–1027.
[13] C.C. Wang, Y.R. Jeng, J.J. Chien, Y.J. Chang, Friction performance of highly viscous fluid in minichannels, Appl. Therm. Eng. 24 (2004) 2243–2250.
[14] B. Agostini, B. Watel, A. Bontemps, B. Thonon, Friction factor and heat transfer coefficient of R134a liquid flow in minichannels, Appl. Therm. Eng. 22 (2002) 1821–1834.
[15] R.S. Downing, G. Kojasoy, Single and two-phase pressure drop characteristics in miniature helical channels, Exp. Therm. Fluid Sci. 26 (2002) 535–546.
[16] R.S. Downing, Analytical and experimental study of single and two-phase cooling in miniature straight and helical channels, Ph.D. Thesis, Department of Mechanical Engineering, University of Wisconsin-Milwaukee, 1999.
[17] F. Debray, J.P. Franc, T. Maitre, S. Reynaud, Measurement of forced convection heat transfer coefficients in minichannels, Mec. Ind. 2 (2001) 443–454.
[18] S. Reynaud, F. Debray, J.P. Franc, T. Maitre, Hydrodynamics and heat transfer in two-dimensional minichannels, Int. J. Heat Mass Transfer 48 (2005) 3197–3211.
[19] B.M. Liu, Y. Mui, Multi-physics simulation of a microprocessor package under water cooling, ASME J. Electron. Packaging 126 (2004) 384–389.
[20] R. Schmidt, Challenges in electronic cooling – opportunities for enhanced – thermal management techniques – microprocessor liquid cooled minichannel heat sink, in: First International Conference on Microchannels and Minichannels, Rochester, NY, 2003, April 24–25.
[21] K. Yazawa, M. Ishizuka, A study of channel optimization in cooling spreader on a smaller and transient heat source, in: Proceedings of Fifth International Conference on Enhanced, Compact and Ultra-Compact Heat Exchangers: Science, Engineering and Technology, Engineering Conferences International, Hoboken, NJ, USA, 2005, September.
[22] S.V. Patankar, Numerical Heat Transfer and Fluid Flow, Hemisphere, NY, 1980.
[23] W.Q. Tao, Numerical Heat Transfer, second ed., Xi'an Jiaotong University Press, Xi'an, China, 2001.
[24] Z.Y. Li, W.Q. Tao, A new stability-guaranteed second-order difference scheme, Numer. Heat Transfer – Part B 42 (4) (2002) 349–365.
[25] Z.G. Qu, W.Q. Tao, Y.L. He, Three-dimensional numerical simulation on laminar heat transfer and fluid flow characteristics of strip fin surfaces with X-arrangement of strips, ASME J. Heat Transfer 126 (4) (2004) 697–707.
[26] D.C. Montgomery, Design and Analysis of Experiments, sixth ed., John Wiley & Son, NY, 2004.
[27] W.Q. Liu, Design of Experiments, Tsinghua University Press, Beijing, China, 2005.
[28] S.J. Kim, D. Kim, Forced convection in microstructures for electronic equipment cooling, J. Heat Transfer 121 (1999) 639–645.
[29] R.W. Knight, D.J. Hall, J.S. Goodling, R.C. Jaeger, Heat sink optimization with application to microchannels, IEEE Trans. Compon. Hybr. Manuf. Technol. 15 (5) (1992) 832–842.
[30] F.P. Incropera, D.P. DeWitt, Introduction to Heat Transfer, third ed., John Wiley & Sons, NY, 1996.